Long-Term Observations of Turbulent Reynolds Stresses over the Inner Continental Shelf

ANTHONY R. KIRINCICH

Woods Hole Oceanographic Institution, Woods Hole, Massachusetts

(Manuscript received 19 August 2012, in final form 10 July 2013)

ABSTRACT

In situ observations of turbulent momentum flux, or Reynolds stresses, were estimated from a 10-yr acoustic Doppler current profiler (ADCP) record of inner-shelf velocities at the Martha's Vineyard Coastal Observatory (MVCO) using recently developed analysis techniques that account for wave-induced biases. These observations were used to examine the vertical structure of stress and turbulent mixing in the coastal ocean during tidal-, wave-, and wind-driven circulation by conditionally averaging the dataset by the level of forcing or stratification present. Bottom-intensified stresses were found during tidally driven flow, having estimated eddy viscosities as high as $1 \times 10^{-2}\,\mathrm{m^{-2}\,s^{-1}}$ during slack water. An assessment of the mean, low-wave, low-wind stress results quantified the magnitude of an unmeasured body force responsible for the mean circulation present in the absence of wind and wave forcing. During weak stratification and isolated wind forcing, downwind stresses matched the observed wind stress near the surface and generally decreased with depth linearly for both along- and across-shelf wind forcing. While consistent with simple models of circulation during across-shelf wind forcing, the linear slope of the stress profile present during along-shelf wind forcing requires the existence of an along-shelf pressure gradient that scales with the wind forcing. At increased levels of stratification, the observed downwind stresses generally weakened and shifted to the across-wind direction during across-shelf and mixed-direction (i.e., onshore and along shelf) wind forcing consistent with Ekman spiral modification, but were more variable during along-shelf wind forcing. No measurable stresses were found due to wave-forced conditions, confirming previous theoretical results.

1. Introduction

This study examines the vertical structure of turbulent stresses present over the inner part of the continental shelf off Martha's Vineyard, Massachusetts due to tidal-, wind-, and wave-driven circulation. Recent works by Fewings et al. (2008) and Lentz et al. (2008) have described the circulation present at the Martha's Vineyard Coastal Observatory (MVCO; Fig. 1), finding significant across-shelf circulation due to across-shelf winds and evidence of wave-driven circulation in the inner shelf. Additional work by Fewings and Lentz (2010) inferred the existence of mean and fluctuating pressure gradients at the site. However, open questions remained regarding the role of stratification and the vertical structure of mixing or momentum transfer on the dynamics and exchange present. Using new methods that allow direct estimates of Reynolds stresses (Kirincich et al. 2010) from in situ ADCP observations in the coastal ocean, this work adds to the description of circulation given by these previous works and tests the correspondence of the observed stresses to simple models of the dynamics due to wave and wind forcing over the inner shelf.

The vertical transfer of momentum due to Reynolds stresses is thought to directly control the magnitude and nature of exchange across the inner shelf (Ekman 1905; Mitchum and Clarke 1986; Lentz 2001). As the surface and bottom boundary layers overlap and interact in this region, the input or removal of momentum by boundary forces is redistributed through the water column via the transport of momentum by turbulent eddies. This transfer of momentum can be represented in the horizontal momentum equations by the turbulent Reynolds stresses:

$$\frac{\partial u}{\partial t} + \mathbf{u}\cdot\nabla u - fv = -\frac{1}{\rho_0}\frac{\partial p}{\partial x} - \frac{\partial}{\partial z}\langle u'w'\rangle \quad \text{and} \tag{1a}$$

$$\frac{\partial v}{\partial t} + \mathbf{u}\cdot\nabla v + fu = -\frac{1}{\rho_0}\frac{\partial p}{\partial y} - \frac{\partial}{\partial z}\langle v'w'\rangle\,, \tag{1b}$$

Corresponding author address: Anthony Kirincich, Woods Hole Oceanographic Institution, 266 Woods Hole Road, Woods Hole, MA 02543.
E-mail: akirincich@whoi.edu

DOI: 10.1175/JPO-D-12-0153.1

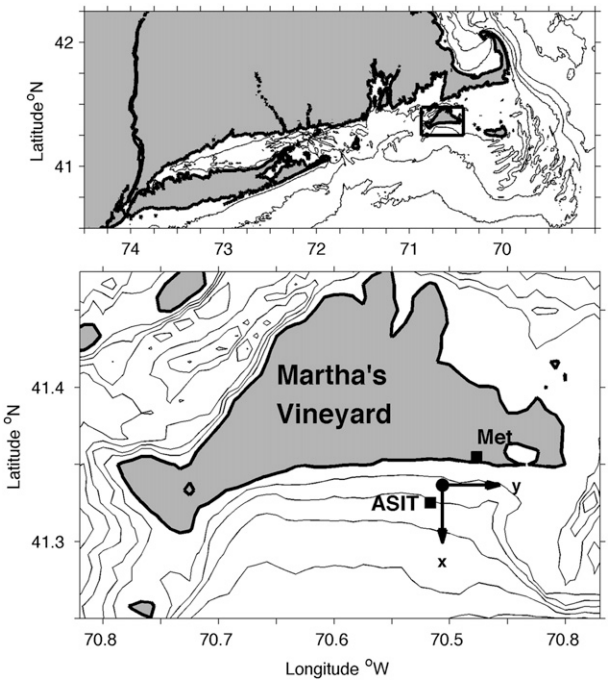

FIG. 1. (top) The southern New England coast of the United States with the inset around Martha's Vineyard, Massachusetts, shown. (bottom) Map of Martha's Vineyard and the MVCO meteorological mast (Met), offshore tower (ASIT), and 12-m underwater node (circle). The along- and across-shelf coordinate system used is shown at the node.

where t is time; p is pressure; and u, v, and w are short time or "burst" mean velocities in the x, y, and z directions with z being the vertical direction, positive upward. Primed quantities denote fluctuations owing to turbulent motions, while angle brackets represent an average over the burst. The vertical divergences of the horizontal Reynolds stresses ($\langle v'w' \rangle$ and $\langle u'w' \rangle$; referred to here as the along- and across-shelf Reynolds stresses), are the last terms in Eqs. (1a) and (1b). The horizontal divergences of Reynolds stresses are generally assumed to be small relative to other terms in areas of uniform forcing and large along-shelf scales (Lentz 1994).

Recent studies of the inner shelf have documented the differing nature of across-shelf exchange present during along-shelf wind forcing (Lentz 2001; Kirincich et al. 2005), across-shelf wind forcing (Tilburg 2003; Fewings 2007), and surface-gravity wave-driven undertow (Lentz et al. 2008; Kirincich et al. 2009), likely due in part to differences in the stress divergence. These potential differences can be illustrated using the unstratified, one-dimensional, eddy-viscosity model developed by Lentz (1995) and expanded to include wave forcing via Xu and Bowen (1994) by Lentz et al. (2008). In steady, along-shelf uniform conditions forced by an along-shelf wind, the dominant balance in the depth-averaged, along-shelf momentum equation is between the wind and bottom stresses (Allen and Smith 1981), and thus the vertical structure of the downwind stress is uniform (Figs. 2a,e). Along-shelf, barotropic pressure gradients can also cause across-shelf exchange (Figs. 2b,f), via a stress profile that increases linearly with depth (Fig. 2b). For across-shelf wind-driven dynamics (Tilburg 2003), an across-shelf pressure gradient balances the across-shelf wind stress and leads to an across-shelf stress profile that linearly decreases with depth (Figs. 2c,g). Wave-driven exchange outside of the surf zone, as documented by Lentz et al. (2008), has the potential to alter observations of the exchange due to other forcings, but is not predicted to cause significant stresses (Figs. 2d,h). As shown here, observations of the Reynolds stresses would offer an expanded picture of dynamics present in coastal flows.

In numerical modeling studies, the contribution of stress in the momentum balance is parameterized using an eddy viscosity A_v as $\langle u'w' \rangle = A_v \partial \overline{u}/\partial z$ (Ekman 1905). While the examples given in Fig. 2 utilized a simple, cubic eddy-viscosity profile, more complex turbulence parameterizations (i.e., Mellor and Yamada 1982; Wilcox 1988) for the effect of the stresses have been developed to account for the role of waves, lateral variability, and stratification in the coastal ocean. In comparative studies, many of the two-equation turbulence closure schemes were found to give similar, quasi-cubic or quasi-bilinear, eddy-viscosity profiles (Warner et al. 2005). Yet, these comparisons, as well as numerous inner-shelf observational (Lentz 1994; Garvine 2004; Munchow and Chant 2000) and modeling (Lentz 1995; Kuebel Cervantes et al. 2003) studies have demonstrated that their exact forms and the structure of the resulting currents were always sensitive to the details of the closure model. Thus, increasing model skill, and therefore our ability to successfully predict the transit of water masses across the shelf, the biological productivity of the coastal ocean and the dispersal or retention of planktonic larvae (Roughgarden et al. 1998), has been limited by our abilities to test these model closures against observations of Reynolds stresses and the eddy-viscosity profiles required to derive the observed velocities.

Observations of Reynolds stresses in the coastal ocean have proven elusive as measurements of interior stresses are easily biased by the effects of surface-gravity waves. However, recent advances in instrumentation and analysis techniques have made it possible to estimate turbulent stresses throughout much of the water column in most shelf environments. These efforts (Trowbridge

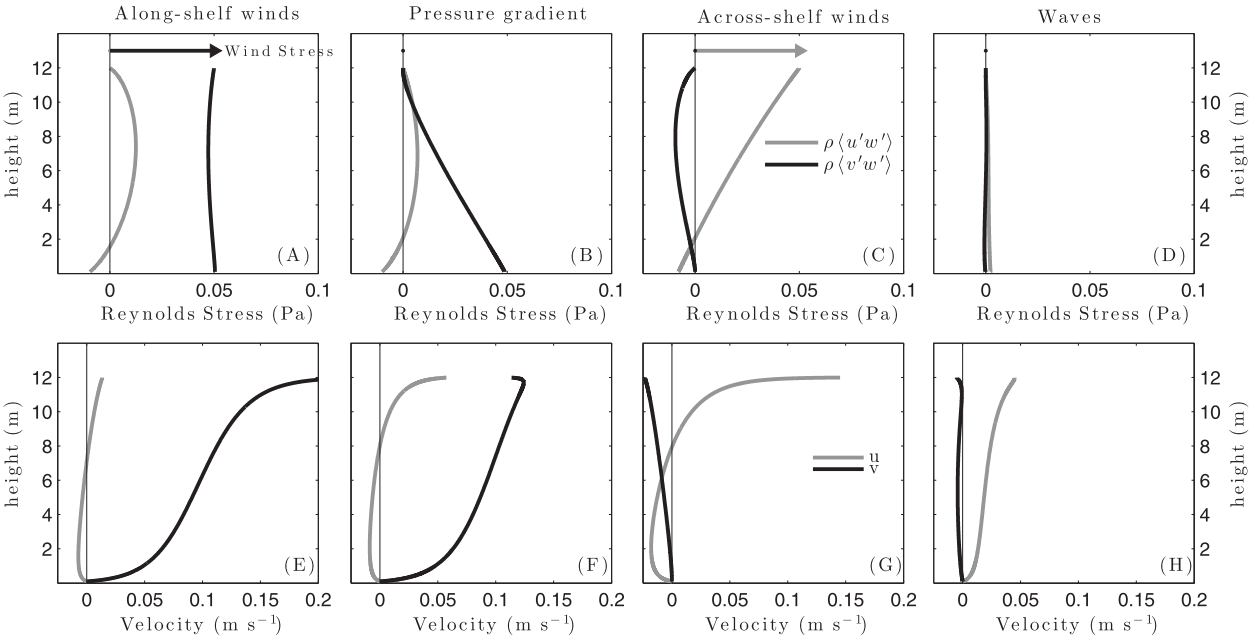

FIG. 2. Model-predicted along- and across-shelf (a)–(d) Reynolds stresses and (e)–(h) velocities due to an along-shelf wind stress of 0.05 Pa in (a),(e); an along-shelf pressure gradient of 4×10^{-6} m s^{-2} in (b),(f); an across-shelf wind stress of 0.05 Pa in (c),(g); and a wave-driven circulation due to a significant wave height H_{sig} of 1 m using the 1D eddy-viscosity model of Lentz et al. (2008) with a cubic eddy-viscosity profile and a roughness coefficient of $z_o = 0.1$ m in (d),(h).

1998; Shaw and Trowbridge 2001; Feddersen and Williams 2007; Gerbi et al. 2008; Rosman et al. 2008; Kirincich et al. 2010; Kirincich and Rosman 2010) have shown that the velocities observed by either acoustic Doppler velocimeters (ADVs) or acoustic Doppler current profilers (ADCPs) can be used to estimate Reynolds stresses by removing the stress biases caused by surface-gravity waves. Thus, estimates of the vertical structure of Reynolds stresses in the coastal ocean are now possible from commonly used instruments capable of long-term deployments.

This study adds to the dynamical picture of inner-shelf circulation at the MVCO described by Fewings et al. (2008), Lentz et al. (2008), and Fewings and Lentz (2010) by examining the role of Reynolds stresses in wind-, wave-, and tidal-driven flows using conditional averages of the long-term observations. Conditional averages are useful for separating the individual effects of wave or wind forcings on the circulation present (Fewings et al. 2008; Lentz et al. 2008) and lessen the effects of increased noise and the reduced data return inherent in the stress calculation, enabling the simple descriptions of inner-shelf circulation (Kirincich and Rosman 2010), presented in Fig. 2 and to be tested using the observed stresses. The manuscript is organized as follows: The MVCO observations and data-processing methods are described first, followed by results for the phase-averaged M_2 tidal response and the background, or mean vertical structure. Next, the vertical structure of Reynolds stress during isolated wave- and wind-forcing conditions is presented for times of weak stratification. The effects of stratification on the vertical structure of stress are then shown for offshore winds, as an example, as well as the overall effects of stratification on the near-surface stress vector. Finally, a dynamical analysis of the stress results is made and the implications of the methodology and results discussed.

2. Observations and methods

a. Observations

This analysis utilizes a 10-yr record of velocity observations obtained by the cabled, underwater node of the Martha's Vineyard Coastal Observatory (MVCO—Fig. 1). Operating since November of 2001, MVCO's underwater node sits in 12 m of water approximately 1.6 km offshore of the island of Martha's Vineyard, Massachusetts. At the node, MVCO operates a bottom-mounted, upward-looking Teledyne RD Instruments 1200-kHz ADCP, which measures velocities from 3.1 m above the bottom to approximately 1 m below the surface at a sample rate of 2 Hz and 0.5-m depth bins using the standard water-pinging mode (mode 1). Profiles of

the raw along-beam velocities during individual 20-min bursts spanning from November 2001 to October 2011 were used to estimate mean horizontal velocities, wave statistics, and Reynolds stresses.

Measurements of wind velocity were made onshore of the node at MVCO Shore Meteorological Station (Met), located 3 km to the north-northeast, and offshore at the Air–Sea Interaction Tower (ASIT), located 1.2 km to the south-southwest (Fig. 1). To maximize the record length of wind observations, a composite wind record was created from the ASIT winds, as they are believed to be most representative of winds at the node, and a modified version of the Met winds when ASIT winds were not available, following Fewings et al. (2008). Wind stress was estimated following the bulk formula of Large and Pond (1981) and assuming neutral conditions. Estimates of bulk wave statistics, including significant wave height, dominant wave period, and incoming wave direction, were calculated from wave spectra derived from the raw ADCP observations following standard methods. While wind forcing varied between winter and summer conditions, wave conditions during these two periods were actually quite similar (Fig. 3).

Estimates of density stratification were available for a limited portion of the velocity dataset from nearby mooring sites deployed as part of the Stratification, Winds, and Waves on the Inner shelf of Martha's Vineyard (SWWIM) program (Lentz et al. 2008) as well as a hydrographic mooring attached to the ASIT tower. SWWIM density observations, consisting of either 5 or 6 Sea-Bird Electronics (SBE)-37 MicroCATs, were available at water depths of 12 and 17 m for approximately three consecutive spring–summer–fall time periods starting in 2007 (Fig. 4). The MVCO ASIT hydrographic chain consisted of 3 SBE-37 MicroCATs located at 2-, 8-, and 14-m depth, and was maintained for 3 months in 2005 and portions of 2008–11. Observations from the SWWIM 12-m mooring were also used to create interpolated density profiles at each of the ADCP bin depths. A time series of top-to-bottom stratification was estimated from the 12-m mooring results and augmented by the 17-m mooring and ASIT hydrochain when data at the 12-m site were not available.

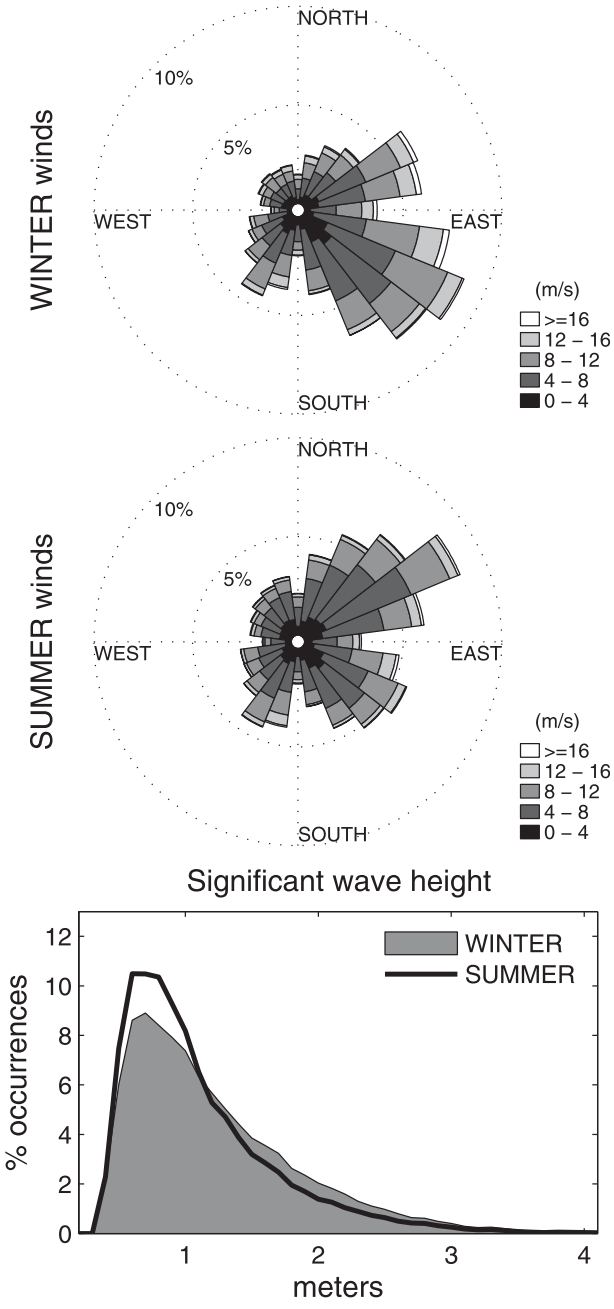

FIG. 3. (top) Wind velocity histograms for the winter (October–March) and summer (April–September) periods of 2001–11, where viable stress estimates (as described in the text) are available. (bottom) Significant wave-height statistics for the winter (shading) and summer (boldface line).

b. Cospectra-fit method stress estimates

Estimates of Reynolds stress were obtained following the cospectra-fit (CF) method (Kirincich et al. 2010; Kirincich and Rosman 2010), which fits a model of the turbulent velocity cospectrum (Kaimal et al. 1972) to the observed cospectrum at wavenumbers greater than those of surface-gravity waves to estimate the total covariance (the Reynolds stress) and the "roll off" wavenumber k_o, a measure of the dominant length scale of turbulent fluctuations. The criteria used to ensure the stress estimates were unbiased and robust (Kirincich et al. 2010) limited reliable estimates of Reynolds stresses to approximately 60% of the available data

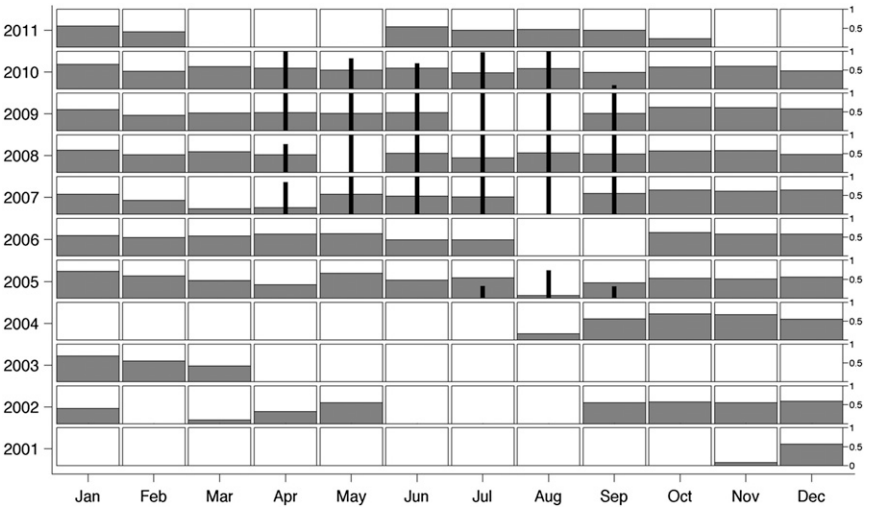

FIG. 4. Monthly fraction of viable stress results from the MVCO 12-m node ADCP dataset. Stress estimates, calculated using the CF method, that did not pass a series of quality-control measures—explained briefly in the text and in Kirincich et al. (2010)—were excluded from further analysis. Availability of summertime stratification estimates, from the SWWIM (Lentz et al. 2008) experiment and the MVCO ASIT hydrographic chain, are shown in the same manner as the boldface line for each potential month.

during weakly stratified conditions and less during more stratified conditions (Fig. 4). However, a number of time periods were eliminated based on poor results of the model fits, velocity shears, and comparisons between the near-bottom stress estimates and quadratic parameterizations of bottom stress using the horizontal velocities. This typically occurred when the faces of the ADCP transducers became heavily fouled toward the end of individual deployments, significantly affecting their performance. These periods include the following: February 2002, June 2002–August 2002, April 2003–July 2004, August and September of 2006, and March 2011–May 2011 (Fig. 4). Stress results were generally available from the bottom-most depth bin, at 3.2-m height, to approximately 1.5 m below the surface or 10.2-m height. A small correction term (Table A1) accounting for the effects of instrument tilt on the estimated stresses, was applied to the resulting time series of stress observations as described in the appendix.

As the ADCP observations were collected using mode 1, instrument noise was a significant issue throughout the analysis. Error estimates of the stress calculation, computed following Kirincich et al. (2010), were similar for both directions and all depth levels, and generally increased from near $1 \times 10^{-4}\,\mathrm{m^2\,s^{-2}}$ for near-zero estimated stresses to approximately $2 \times 10^{-4}\,\mathrm{m^2\,s^{-2}}$ for stresses $2 \times 10^{-4}\,\mathrm{m^2\,s^{-2}}$ or greater (Fig. 5). These error estimates were an order of magnitude higher than that possible using lower ADCP noise sampling modes such as mode 12 (Nidzieko et al. 2006; Rosman et al. 2008).

c. *Analysis preparation*

The velocity and stress results were rotated into an across- and along-shelf coordinate system defined by the principle axis of the depth-averaged, subtidal velocity during low-wind and low-wave conditions, following Lentz et al. (2008) and Fewings et al. (2008). Hourly averaged stress and velocity observations from only those times/depths when viable stress estimates were available were interpolated using a spline fit to fill in gaps between the top and bottom available observations and reduce the effect of noise on each individual profile, following Stacey et al. (1999a). A spline-smoothing factor of 0.8 was found, by inspection, to eliminate obvious spikes while preserving the overall shape of the profile. An estimate of the eddy viscosity was computed from the hourly averaged stress and velocity shear in the along-shelf direction as $A_v = \langle v'w' \rangle / (\partial v / \partial z)$ to aid the examination of the tidal and mean or background dynamics. Similar estimates from the across-shelf stresses and shear had higher noise levels and were generally not significantly different than zero.

Despite use of the composite time series of stratification, little data were available during winter months when stratification was likely the weakest and the stress estimates most often viable (Kirincich et al. 2010). Based on inspection of the available stratification during winter, a weak stratification—described here using the buoyancy frequency—of $2 \times 10^{-3}\,\mathrm{s^{-1}}$ was assumed for all data between the months of October and March.

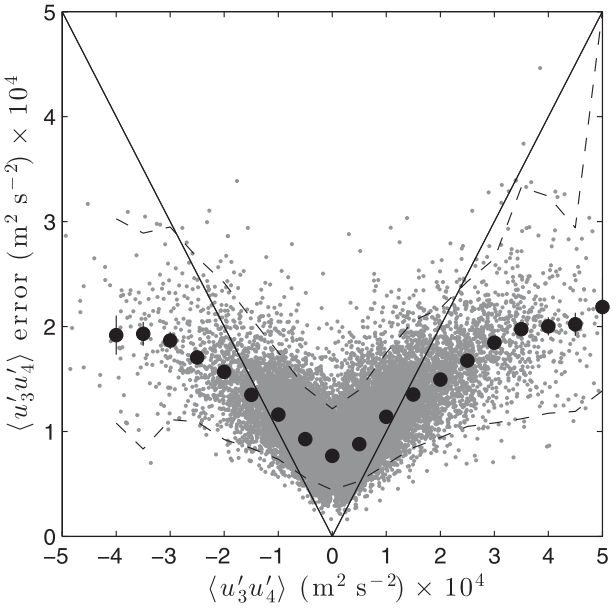

FIG. 5. Uncertainty estimates for stresses derived using the CF method in depth-bin 10 (7.7-m height) along the 3–4 instrument axis (gray), which was representative of uncertainties in both directions and all depths. Bin averages for bins $5 \times 10^{-5}\,\mathrm{m^2\,s^{-2}}$ wide (black circles) with standard error bounds (generally smaller that the size of the circle), and the 2.5% and 97.4% limits of the distributions for each bin average (dashed lines). The 1–1 lines are included (solid) for reference.

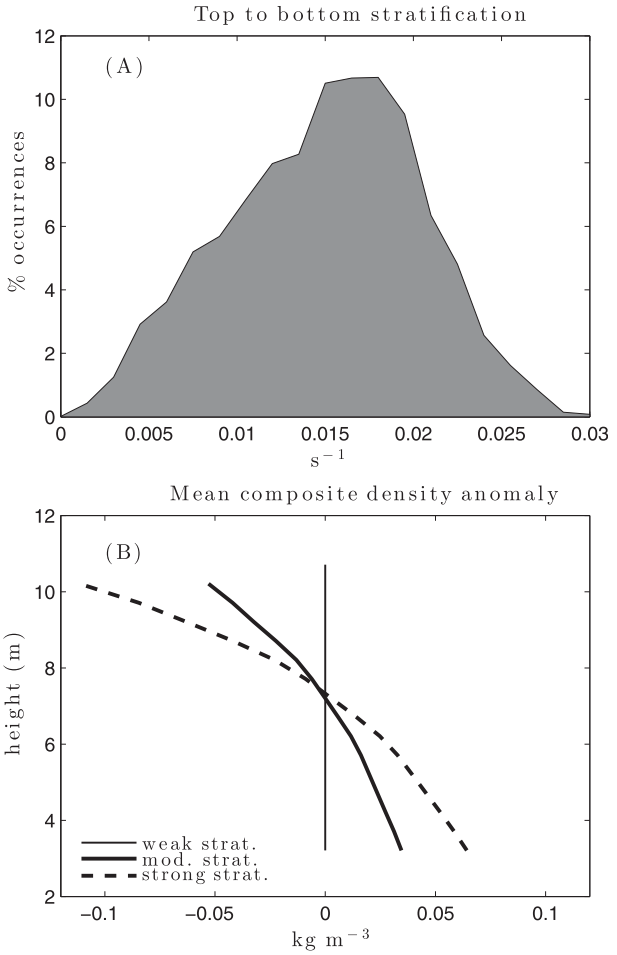

FIG. 6. (a) Histogram of all available summer buoyancy frequency N estimates, as described in the text. (b) Mean density anomaly profiles for weak (from 0 to $2.2 \times 10^{-3}\,\mathrm{s^{-1}}$), moderate (from 2.2×10^{-3} to $0.015\,\mathrm{s^{-1}}$), and strong (from 0.015 to $0.025\,\mathrm{s^{-1}}$) stratification.

During the summer months (May–September) where stratification estimates were available, estimates varied significantly at subtidal time scales. While maximum values as high as $0.03\,\mathrm{s^{-1}}$ were observed, stratification was generally less than $0.022\,\mathrm{s^{-1}}$ (Fig. 6a). Based on the stratification distribution, and the occurrences of viable stress estimates, three levels of stratification were chosen for examination here: weakly (from 0 to $2.2 \times 10^{-3}\,\mathrm{s^{-1}}$), moderately (from 2.2×10^{-3} to $0.015\,\mathrm{s^{-1}}$), and strongly (from 0.015 to $0.025\,\mathrm{s^{-1}}$) stratified, with the mean vertical structure of each shown in Fig. 6b.

This analysis focuses on conditional averages of the vertical structure present during isolated tidal-, wave-, or wind-driven dynamics. However, many of the conditional averages had small sample sizes relative to the total record length (Table 1) such that the tides had a significant effect on the mean standard error estimates of the velocity and stress profiles. Thus, before computing the wave- and wind-driven conditional averages, tidal fits to the velocities and stresses were estimated using T_tide (Pawlowicz et al. 2002) and subtracted from the hourly averaged time series. Finally, to minimize the effect of outliers on the average results shown, all bin averages and standard errors were computed as the mean value and standard deviation of the middle 90% of the distribution. Standard errors were estimated using effective degrees of freedom, following Chelton (1983).

TABLE 1. Sample sizes (h) for each wind-driven conditional average described in the text. Degrees True are indicated by °T.

Wind direction bearing (°T)	Stratification		
	Weak	Moderate	Strong
180°	279	49	32
90°	303	47	69
0°	149	65	97
270°	129	101	27
150°	705	34	51
50°	262	175	218
200°	336	96	38

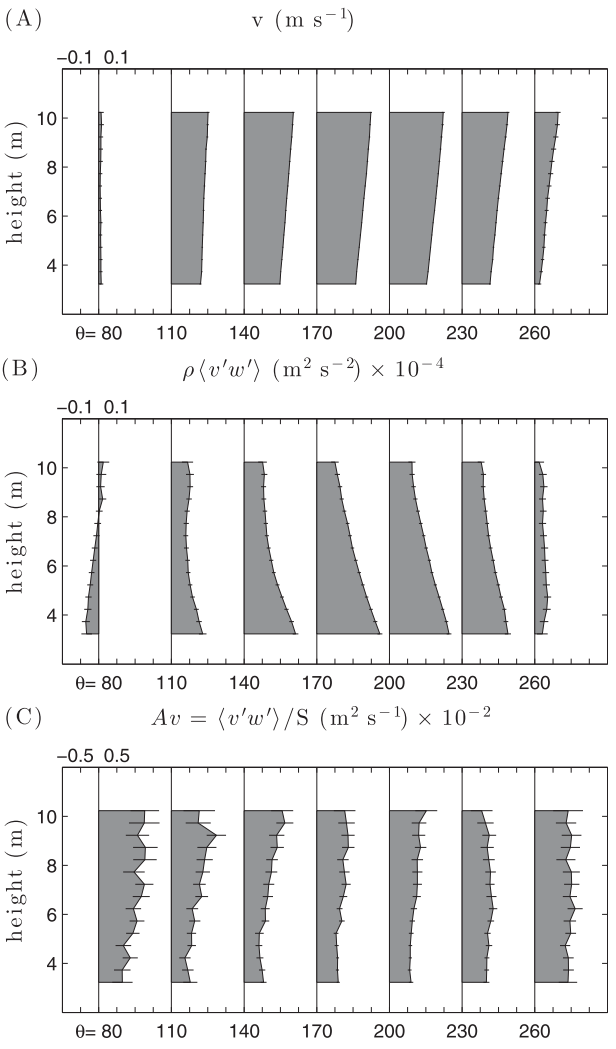

FIG. 7. Phase-averaged along-shelf (a) velocity, (b) Reynolds stress, and (c) and eddy viscosity for seven 30°-wide phase bins of the M_2 tide starting at $\theta = 80$. Standard error bars for the bin averages are shown at each depth for all phase averages and S is the along-shelf velocity shear.

3. Results

a. Tidally averaged stresses

Accounting for more than 70% of the variance of the hourly averaged velocity observations at MVCO, the M_2 tidal constituent was the dominant component found, with depth-dependent semi-major velocity amplitudes of 0.2–0.3 m s^{-1}. The phase-averaged along-shelf velocity, stress, and eddy-viscosity profiles from one-half of the tidal cycle (Fig. 7) illustrate the tidally driven changes in the magnitude and vertical structure that occur between subsequent slack water periods. At maximum tidal velocity ($\theta = 170$ in Fig. 7a), M_2 phase-averaged stresses were a maximum of 3.5×10^{-5} m^2 s^{-2} at 3-m height and decreased linearly to 1×10^{-5} m^2 s^{-2} at ~2 m below the surface. While the stress was bottom intensified both approaching and departing from the time of maximum velocity (θ = 110, 140, and 230; Fig. 7b), local minima existed in the middle of the water column most notably on the approach to maximum velocity. Standard errors of both the velocity and stress estimates were highest near times of slack water, indicating variability in the vertical structure and/or timing of the change in direction. Eddy viscosities were largest at times of slack water (θ = 80 and 260; Fig. 7c), with near surface values from 1×10^{-2} to 1.5×10^{-2} m^2 s^{-1}. The vertical structure of eddy viscosity was surface intensified during the approach to maximum velocity and more depth uniform between the time of maximum velocity and the next slack water. This vertical structure contrasts with that predicted for an along-shelf flow driven by a pressure gradient, as will be shown in section 5.

b. Low-wind, low-wave mean conditions

The background, or mean vertical structures of velocity, stress, and along-shelf eddy viscosity during low wind and wave conditions were found by averaging all observations with $|\tau^{\mathbf{w}}| < 0.03$ Pa and $H_{\text{sig}} < 0.75$ m (Fig. 8). A total of 2712, 770, and 740 hourly observations were used to compute the mean profiles for the weak, moderate, and strong stratification, respectively. As was found by Fewings and Lentz (2011) and Lentz et al. (2008), the mean along-shelf velocities were westward and near 0.06 m s^{-1} during the weakly stratified winter months (Fig. 8a), but increased in speed and vertical shear as stratification increased (Figs. 8f,k). Across-shelf velocities were offshore at the surface and near zero at depth for all stratification levels, although the shear and the magnitude of the offshore flow increased with stratification (Figs. 8b,g,l). Despite $H_{\text{sig}} <$ 0.75 m for all levels of stratification, much of the vertical structure and magnitude of the across-shelf velocity, particularly during weak stratification, can be explained by the Eulerian response to wave forcing, as will be described in section 3c.

In general, the low-wind, low-wave mean stress profiles were small. Mean stresses in the along-shelf direction (Figs. 8c,h,m) were bottom intensified, westward, and decreased from 0.04 to 0.03 Pa approximately linearly with height toward the mean wind stress near the surface. The slope of the along-shelf stress increased with increasing levels of stratification. Estimated mean stresses in the across-shelf direction were generally smaller, near 0.01–0.015 Pa, and more uniform with depth than the along-shelf stresses (Figs. 8d,i,n). Near-surface stresses were similar, within the confidence intervals shown, to the mean wind stresses. The corresponding

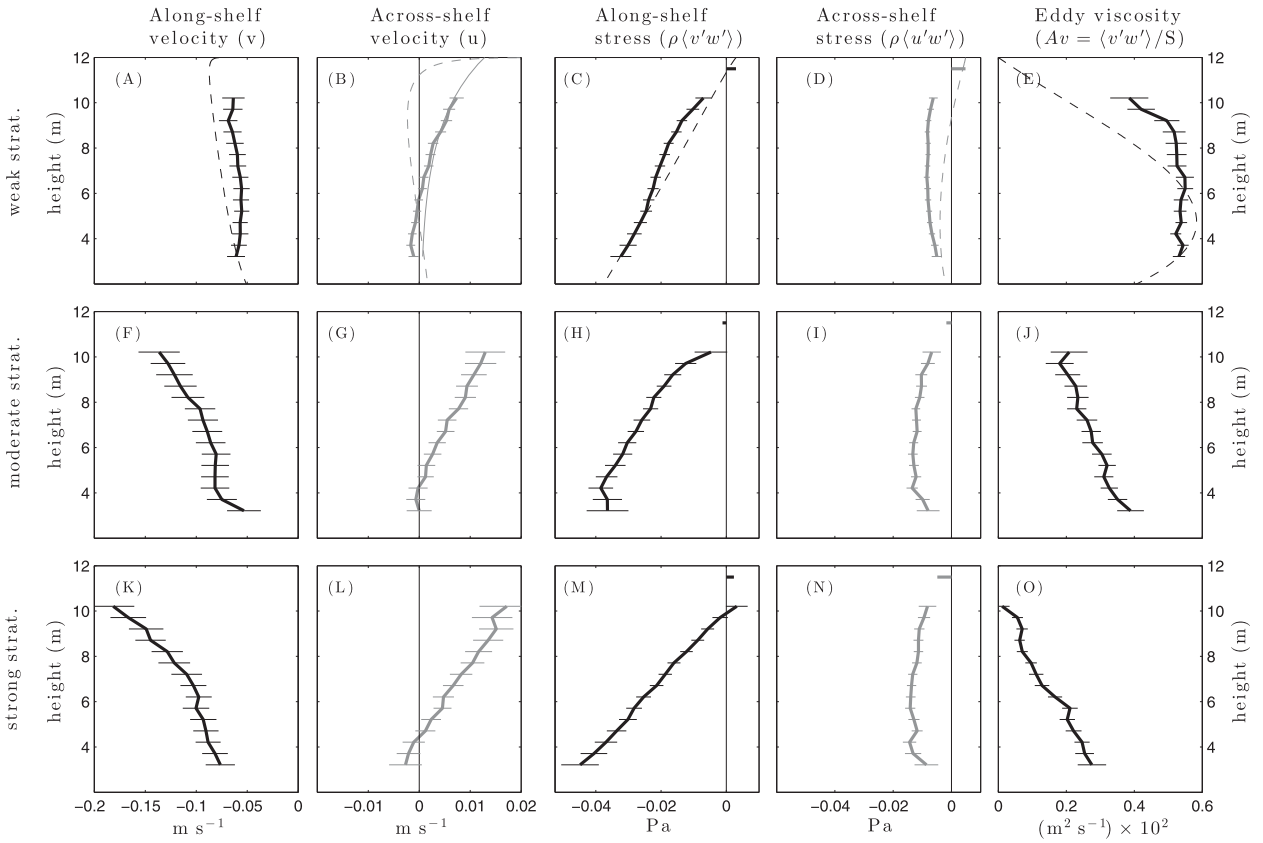

FIG. 8. Conditionally averaged (a),(f),(k) along-shelf velocity; (b),(g),(l) across-shelf velocity; (c),(h),(m) along-shelf stress; (d),(i),(n) across-shelf stress; and (e),(j),(o) along-shelf eddy viscosity during low-wave ($H_{sig} < 0.75$ m) and low-wind ($|\tau^{w}| < 0.03$ Pa) conditions for each of the three stratification levels described in Fig. 6. The mean wind stresses are shown for each direction and stratification level as horizontal lines above 11-m height in (c),(d),(h),(i),(m),(n). As described in section 5, the predicted wave-driven return flow in (b) (thin solid line) and (top) the results of a 1D model (Lentz 1995; Lentz et al. 2008) forced by a 4×10^{-6} m s^{-2} along-shelf pressure gradient (dashed lines) are included for the mean profiles during times of weak stratification.

mean eddy-viscosity profile for weak stratification was approximately constant with depth between 3- and 9-m height, at 0.55×10^{-2} m^2 s^{-1}, but decreased sharply near the surface (Fig. 8e). At increased levels of stratification, eddy viscosities were reduced in magnitude and bottom intensified, decreasing approximately linearly with height (Figs. 8j,o).

c. *Wave-driven conditions*

Recent work by Lentz et al. (2008) has shown that a portion of the Eulerian across-shelf velocities observed at MVCO was due to a return flow associated with the onshore wave-driven Stokes drift. Following Lentz et al. (2008), the vertical structure of this return flow is determined by the intensity of turbulent mixing present: parabolic at high levels of wave-driven turbulence, generally assumed to exist onshore near the surf zone, and surface intensified at low levels of wave-driven turbulence, due to the Stokes–Coriolis force (or Hasselmann wave stress). Lentz et al. (2008) found that the velocity structure during wave forcing at the MVCO was surface intensified, and thus inferred that flow was driven by the Stokes–Coriolis force and that turbulence, or the Reynolds stress, was weak during isolated wave-driven flow. As shown in Fig. 8b, the predicted Stokes–Coriolis return flow, based solely on the mean significant wave height and dominant wave period, estimated using Eqs. (7) and (8) of Lentz et al. (2008), matches the vertical structure and magnitude of the observed mean velocity profile during weakly stratified conditions.

However, the estimated Reynolds stresses offer a more direct way to test the conclusion reached by Lentz et al. (2008), as the low-turbulence conditions, $A_v < 10^{-4}$ m^2 s^{-1}, that would result in a surface-intensified, wave-driven return flow would correspond to stresses far below the noise levels of the observed stresses. Thus, the absence of stress relative to the magnitude of the across-shelf velocities observed during times of isolated wave forcing could be the result of the wave-driven circulation described by Lentz et al. (2008). Times of weak

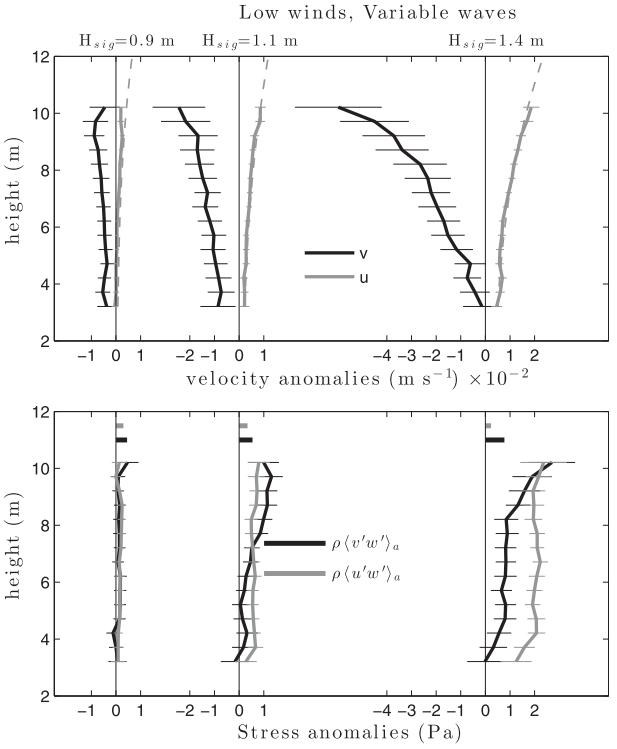

FIG. 9. (top) Velocity and (bottom) Reynolds stress anomalies caused by increasing H_{sig}, defined as the differences of conditional averages for low winds but increasing levels of H_{sig} from the low-wind, low-wave conditional averages shown in Fig. 8. The mean H_{sig} for each wave-height bin are given above each velocity profile, as are the theoretical Stokes–Coriolis wave-driven return flow (gray dashed), following Lentz et al. (2008). Across- (gray) and along-shelf (black) wind stresses are shown as horizontal bars above 11-m height in the bottom panel. The number of hourly results used in each bin average was 774, 398, and 255 for the 0.9-, 1.1-, and 1.4-m bins respectively.

stratification and weak wind forcing (<0.03 Pa) within the dataset were conditionally averaged by H_{sig} into three groups with ranges of 0.75–1, 1–1.25, and 1.25–1.75 m. Then, the low-wind-, low-wave-average profiles described above, having $H_{sig} < 0.75$ m, were subtracted from the conditionally averaged velocity and stress profiles at higher levels of wave forcing to separate the incremental effects of increasing wave heights from the background vertical structure described above.

The resulting velocity and stress profiles (denoted in Fig. 9 and others with a subscript *a*) represent anomalies from the low-wave, low-wind means and document the change in conditions purely because of increased wave forcing. For $H_{sig} = 0.9$ m, the stress anomalies were small, at 2.5×10^{-3} Pa, vertically uniform, and matched the magnitude of the mean wind stresses present for both the along- and across-shelf directions (Fig. 9, lower panel). With increasing levels of significant wave height, the stresses in the along-shelf direction (black lines) increased in magnitude along with the mean wind stress but exceeded the winds above a height of 8 m. Across-shelf stresses (gray lines) remained vertically uniform for all levels, and were significantly different from the mean wind stress only for wave heights of 1.4 m, where they were 4 times greater than the wind stress. The conditionally averaged across-shelf velocity anomalies were vertically sheared and surface intensified for all wave-height bins (Fig. 9, upper panel, solid gray lines), and agreed closely with theoretical estimates (Lentz et al. 2008) for the across-shelf velocity anomalies driven by the Stokes–Coriolis wave stress (upper panel, dashed gray lines). For consistency, the theoretical estimates were shown as anomalies from the theoretical estimate for the mean low-wind, low-wave conditions (Fig. 8b). Observed along-shelf velocities (black lines) also increased in magnitude with wave height and oppose the direction of the mean wind forcing. The implications of these observations are discussed in section 5.

d. Wind-driven stresses

This section describes the vertical structure of velocities and Reynolds stresses present during moderate wind forcing, defined here as the middle third of the wind stress distribution, or 0.03–0.07 Pa. Conditionally averaged results were found for times of $H_{sig} < 1.25$ m and winds directed $<\pm 15°$ from the along- or across-shelf directions, referred to here as ''on axis'' winds, and for the dominant wind-forcing directions at the study area: 50°, 150°, and 200°T (Fig. 3), referred to here as ''off axis'' winds, for each of the three stratification levels described above. Sample sizes for 1each of the wind-driven conditional averages considered are given in Table 1. As done above, the low-wind mean velocities and stresses for each stratification level were subtracted from the conditional averages at moderate wind forcing, and the resulting velocity and stress anomalies were used to isolate the wind-driven component of the circulation. The correspondence of the near-surface, down-wind stress anomalies to the observed wind stress and the observed vertical structure for moderate winds were representative of conditional averages for both weaker and stronger levels of wind forcing.

1) WEAK STRATIFICATION

For across-shelf wind forcing during weak stratification, across-shelf velocities were downwind near the surface, and upwind at depth with magnitudes up to 0.01 m s^{-1} and zero-crossings near 8-m height (Figs. 10a,b). Along-shelf velocities were uniform with depth, to the right of the wind direction, and maximum values of 0.015 m s^{-1}. Across-shelf Reynolds stress anomalies during across-shelf wind forcing matched the magnitude

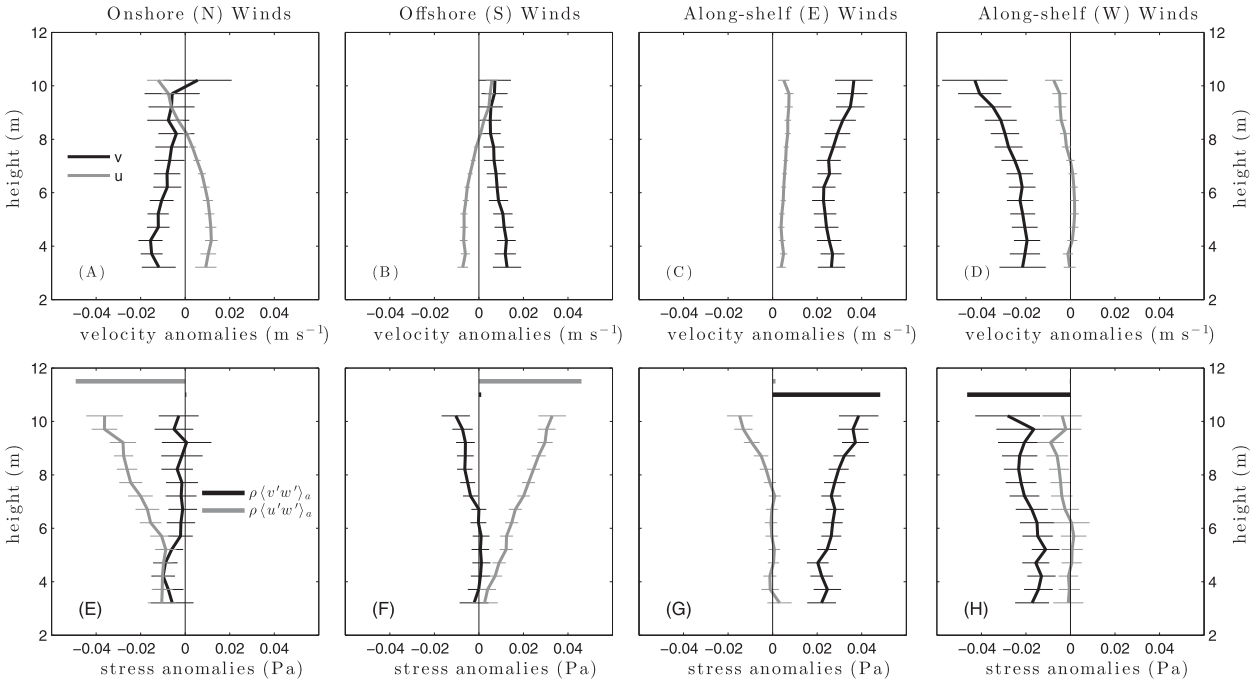

FIG. 10. (a)–(d) Velocity and (e)–(h) Reynolds stress anomalies during times of moderate onshore/northward winds in (a),(e); offshore/southward winds in (b),(f); along-shelf/eastward winds in (c),(g); and along-shelf/westward winds in (d),(h); defined as the differences of conditional averages for moderate winds and low waves from the low-wind, low-wave conditional averages shown in Fig. 8. In each panel, along- (black) and across-shelf (gray) velocities or stresses are shown along with standard error bounds. Mean wind forcing is shown as the horizontal bars at 11- or 11.5-m height in (e)–(h).

of the mean winds near the surface, and decreased linearly with depth toward zero stress at the bottom (Figs. 10e,f), consistent with 1D model predictions (Fig. 2f). Along-shelf stresses were near zero or slightly negative for both positive and negative across-shelf winds.

For along-shelf wind forcing, along-shelf velocities were vertically sheared, increasing to 0.04 m s^{-1} near the surface (Figs. 10c,d). Across-shelf velocities were generally weak, $<7.5 \times 10^{-3}$ m s^{-1} and all positive (offshore) for eastward winds but onshore at the surface and offshore with depth for westward winds. Along-shelf stresses were similar to the wind stress at the surface but decreased linearly with depth (Figs. 10g,h) for both directions, and thus were inconsistent with the constant stress profile predicted by the along-shelf uniform 1D model (Fig. 2e). Across-shelf stresses were similar for both wind directions, near zero below 7-m height and increasing above that depth to -0.01 Pa at 10.5 m.

While strictly along- or across-shelf wind forcing has been the primary focus of most dynamical studies, the dominant winds at MVCO were from the northwest during winter, with an approximate oceanographic bearing of 150°T, but also toward 50°T and 200°T, and from the southwest during summer or toward 50°T (Fig. 3). For wind stresses toward 50°T or toward the northeast (onshore and upwelling favorable), across-shelf velocity anomalies were offshore throughout the measured portion of the water column but reached zero at 10-m height, suggesting that onshore (negative) velocity anomalies were likely above this level (Fig. 11a). Along-shelf velocities were eastward, surface intensified with velocities up to 0.03 m s^{-1}. Stress anomalies for both the across- and along-shelf components were surface intensified and decreased linearly toward zero with depth (Fig. 11d), although the along-shelf stress was only half the observed wind stress near the surface. For wind stresses toward 150°T, or offshore and upwelling favorable, the across-shelf component of the wind stress dominated the velocity and the stress response (Figs. 11b,e). Across-shelf velocity anomalies were offshore above 8-m height and up to 5×10^{-3} m s^{-1} onshore at depth while along-shelf velocities were near 0.03 m s^{-1} and eastward (Fig. 11b). The across-shelf stress anomalies decreased linearly from the wind stress at the surface toward zero with depth while the along-shelf stress anomaly was more vertically uniform (Fig. 11e). Finally, for wind stresses toward 200°T, across-shelf velocities were slightly offshore above 9-m height, but onshore at depth while along-shelf velocities were westward and surface intensified up to 0.025 m s^{-1} (Fig. 11c). Both the along- and across-shelf stress profiles

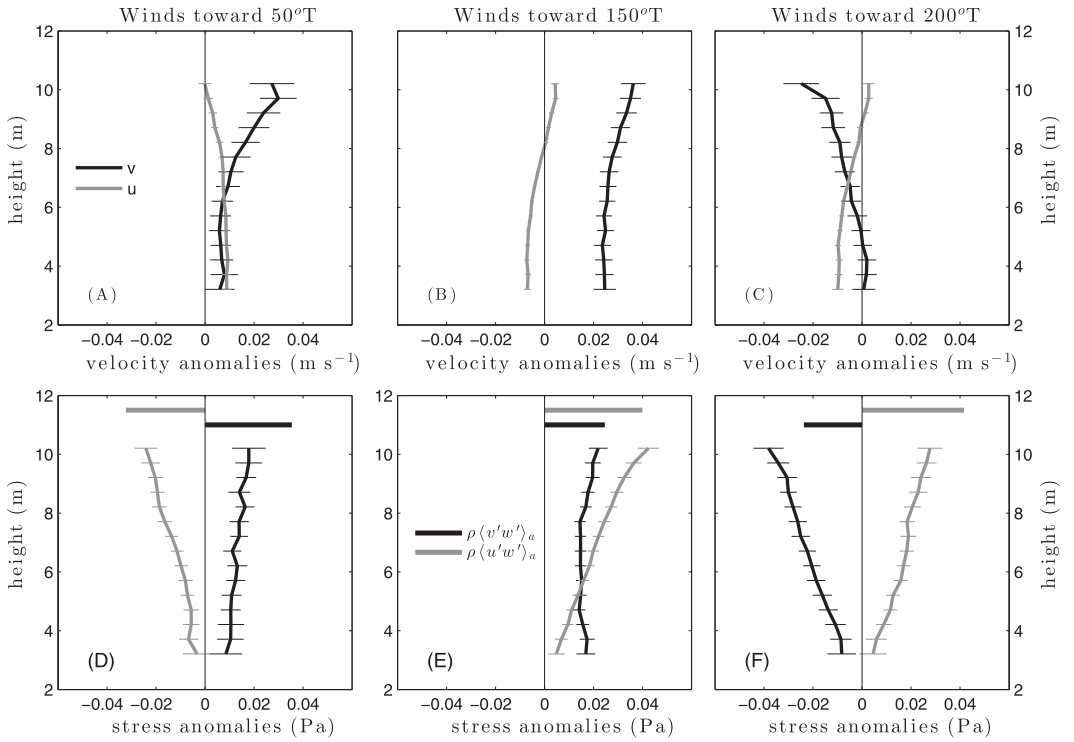

FIG. 11. As in Fig. 10, but for conditionally averaged (a)–(c) velocity and (d)–(f) stress anomalies during times of moderate wind forcing toward 50°T in (a),(d); 150°T in (b),(e); and 200°T in (c),(f).

decreased linearly with depth (Fig. 11f), although the along-shelf stress was larger than the wind stress near the surface. Thus, for off-axis wind forcing, the vertical structure of both stress components tended to decrease with depth, with the exception of the along-shelf stress for winds toward 150°T.

2) INCREASED STRATIFICATION

The effect of stratification on the vertical structure of the velocity and stress anomalies can be seen in the velocity and stress anomalies during onshore (negative across shelf) winds. While the maximum across-shelf velocities do not vary significantly with stratification, the zero crossing of the across-shelf velocity profile increased from 8- to 10-m height as stratification increased (Fig. 12). Along-shelf velocity profiles, westward and bottom intensified for weak stratification, become surface intensified and eastward as stratification increases. Across-shelf stress anomalies, which decreased with depth from the wind stress toward zero over the water column for weak stratification, became reduced and more surface intensified as stratification increased (Fig. 12). Along-shelf stresses in the top 6 m, which were near zero for weak stratification, became increasingly positive as stratification increased.

The changes in velocity and stress anomalies with increased stratification observed during onshore winds (Fig. 12) were not representative of the anomalies found during other wind directions. Comparisons of the near-surface, ~1.8-m depth, stress anomaly vectors at all levels of stratification to the wind stress vector for each of the seven wind directions considered in Figs. 10 and 11, reveal a variety of responses with increased stratification for along- and across-shelf winds. The near-surface stress results, and not the velocity results, were focused on here as, due to the zero crossing of the across-shelf velocity profiles that occurs near this depth (i.e., Figs. 10a,b), changes in the orientation and magnitude of the velocity vector as stratification increased were small and difficult to observe definitively.

For isolated across-shelf wind forcing, near-surface stress anomaly vectors during weak stratification were directed downwind (±10°), but rotated up to 45° to the right of the wind as stratification increased (Figs. 13a,b). A similar rotation from downwind to up to ~45° to the right of the wind was found for winds toward 150°T (Fig. 13f). However, near-surface stress vectors during along-shelf winds followed the wind direction closely for westward winds (Fig. 13d) and when the along-shelf component of the wind stress was significant during mixed wind conditions (i.e., winds toward 50°T; Fig.

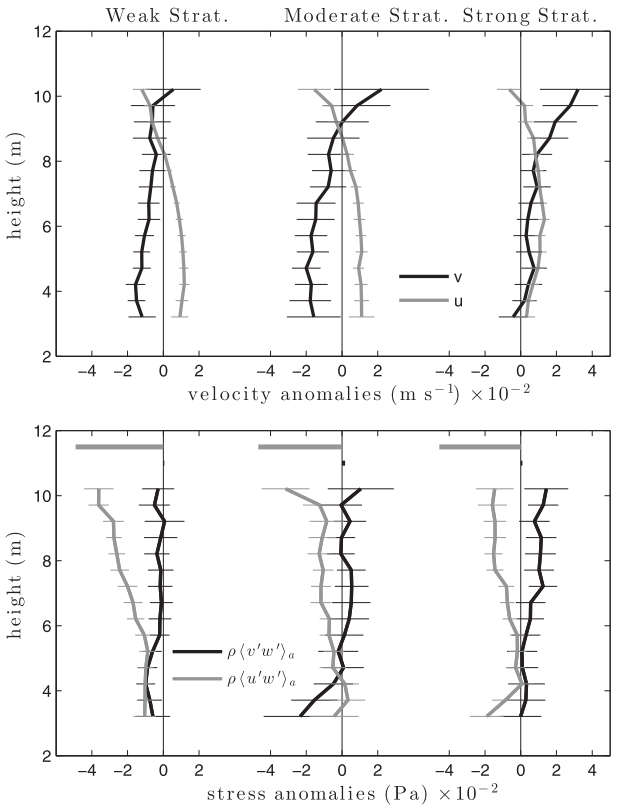

FIG. 12. Conditionally averaged (top) velocity and (bottom) Reynolds stress anomalies—as defined in the text—during moderate onshore (negative across-shelf) wind forcing and increasing levels of stratification. Across- (gray) and along-shelf (black) velocities/stresses are shown with standard error bars at each bin depth along with the conditional-average's mean wind stress, as horizontal bars above 11-m height in the bottom panel.

13e). Stress vectors during along-shelf (eastward) winds were to the left of the wind during weak and moderate stratification, and near zero for strong stratification (Fig. 13c). Winds toward 200°T result in similar stress directions for all levels of stratification, approximately 30° to the right of the wind.

The rotation of stress anomaly vectors to the right of the wind with increased stratification, up to 45°, coupled with the decreased stress magnitude seen during dominant across-shelf wind forcing is consistent with a shoaling surface boundary layer, causing the stress observations from a fixed depth to sample a different portion of the Ekman spiral. When along-shelf winds were dominant, or equal in magnitude to the across-shelf winds (Fig. 13), stresses were essentially downwind for all levels of stratification. This pattern is not entirely inconsistent with the idea of a shoaling Ekman spiral as long as the boundary layers still overlap significantly. While compressing, or vertically shifting the theoretical stress profile for across-shelf winds shown in Fig. 2c causes a sizable difference in angle of the stress relative to the wind, a similar shift for along-shelf winds shown in Fig. 2c would not cause a significant difference in angle. This result suggests that the model prediction of stress and velocities shown in Fig. 2c might not change significantly with increasing stratification at these shallow water depths. However, a key unknown is understanding the cause of the surface-intensified stress profiles found for along-shelf wind forcing, which disagree with the simple model prediction, and determining if this forcing is present during times of increased stratification as well. Finally, the differences found among the off-axis wind-forcing results shown might be due to the relative contribution of coastal up- and downwelling by the along- and across-shelf wind components. Both components are upwelling favorable for winds toward 150°T, but the effects of the components tend to oppose each other for winds toward 50° and 200°T.

4. Dynamical assessment

The results presented above link the velocity structures observed in response to common forcing events to the corresponding Reynolds stress profiles and provide the opportunity to explore the dynamics of circulation present in a new way. This section uses the stress results to examine the role of along-shelf pressure gradients in along-shelf wind-driven dynamics and tests the mean momentum budgets for the MVCO dataset as well as the wave-driven circulation inferred in previous works.

a. Diagnosing along-shelf pressure gradients

The linearly decreasing vertical structure of the along-shelf stress during along-shelf wind forcing (Figs. 10 and 11) is not characteristic of the simple, along-shelf uniform momentum balance illustrated in Fig. 2. Additionally, the along-shelf stress profiles have slopes that increase with increasing wind stress (Fig. 14a). These results suggest that an along-shelf pressure gradient that scales with the magnitude of the wind forcing could account for the difference shown.

Estimates of the terms in the along-shelf momentum balance [Eq. (1b)] are necessary to test this hypothesis. The magnitude and vertical structure of the Coriolis, Reynolds stress, and two of the three advective terms in Eq. (1b), the across-shelf flux of along-shelf momentum and the vertical flux of along-shelf momentum, were estimated following Lentz (2001) using the velocity and stress anomaly profiles for moderate along-shelf wind forcing and weak stratification and are shown in Fig. 14b. Following Lentz et al. (1999) and Kirincich and

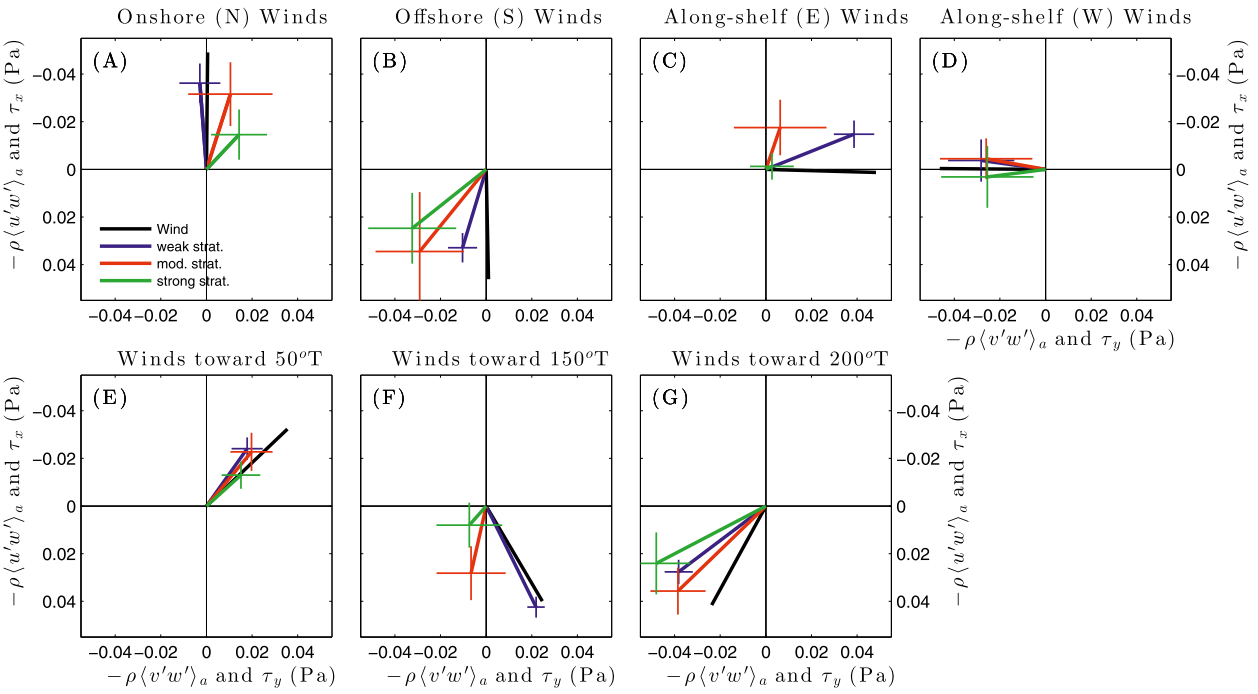

FIG. 13. Wind and near-surface (1.8-m depth) stress anomaly vectors for moderate wind forcing in each of the seven conditionally averaged wind directions considered in Figs. 10 and 11 for weak (blue), moderate (red), and strong (green) stratification levels. Note that the coordinate system is reversed such that true north, the direction of negative across-shelf (onshore) velocities, is oriented upward for visual convenience.

Barth (2009), estimates of the two nonlinear terms assumed a coastal boundary condition inshore ($u = 0$ at the coast), enabling an estimate of $\partial u/\partial x$, and that the vertical velocity had a parabolic structure and a maximum value that matched the observed across-shelf transport. The third nonlinear term, the along-shelf flux of along-shelf momentum could not be estimated with the data at hand. However, scaling analysis indicated that its magnitude was likely the same or less than the other nonlinear terms. Errors bars for the Coriolis term assumed an upper bound of $5 \times 10^{-3}\,\mathrm{m\,s^{-1}}$ for the error of the temporally averaged velocities. Error bars for the slope of the Reynolds stress anomalies were based on the error bounds of the linear fit to the stress profile. Because of the coarse assumptions used in their estimate, true error bounds were not readily available for the nonlinear terms.

Comparing the magnitude and vertical structure of all measured terms (Fig. 14b) finds that the stress term dominates. The largest of the estimated nonlinear terms, the across-shelf flux of along-shelf momentum was small, at less than $0.2 \times 10^{-6}\,\mathrm{m\,s^{-2}}$. The Coriolis term was only slightly larger at up to $0.6 \times 10^{-6}\,\mathrm{m\,s^{-2}}$. In contrast, the linear regression to the observed Reynolds stress anomalies required a momentum input of $2.5 \times 10^{-6}\,\mathrm{m\,s^{-2}}$, much larger than any of the other terms estimated. The only term remaining in Eq. (1b) was the along-shelf pressure gradient, suggesting that it must vary to oppose the along-shelf stresses (Fig. 14b). Similar results exist for the low- and high-wind-forcing levels.

A comparison of the depth-averaged mean residual momentum for each wind level against the mean wind stress observed for the level (Fig. 14c) gives an approximate relationship between the wind stress forcing and what can be assumed to be a coupled pressure gradient response. A linear fit of the trend between the observed winds and the residual momentum had a slope of $5.5 \times 10^{-4}\,\mathrm{m\,s^{-2}\,Pa^{-1}}$. If the residual momentum was indeed due to a pressure gradient, the residual would require a pressure gradient of $2.8 \times 10^{-3}\,\mathrm{Pa\,m^{-1}}$ during a wind forcing of 0.05 Pa. Recasting Fig. 14c using the wind and pressure terms in the depth-averaged momentum equation, the slope of the linear fit would be 0.8 ± 0.6, similar to the 0.9 ± 0.4 inferred by Fewings and Lentz (2010) using regressions between the wind stress and observed pressure. Thus, an important result of this analysis is that the observed stresses can be used to infer an unmeasured pressure gradient if the nonlinear terms are small.

Expanding this comparison for all times when the wind was along-shelf, having bearings of 90° ± 15°T or

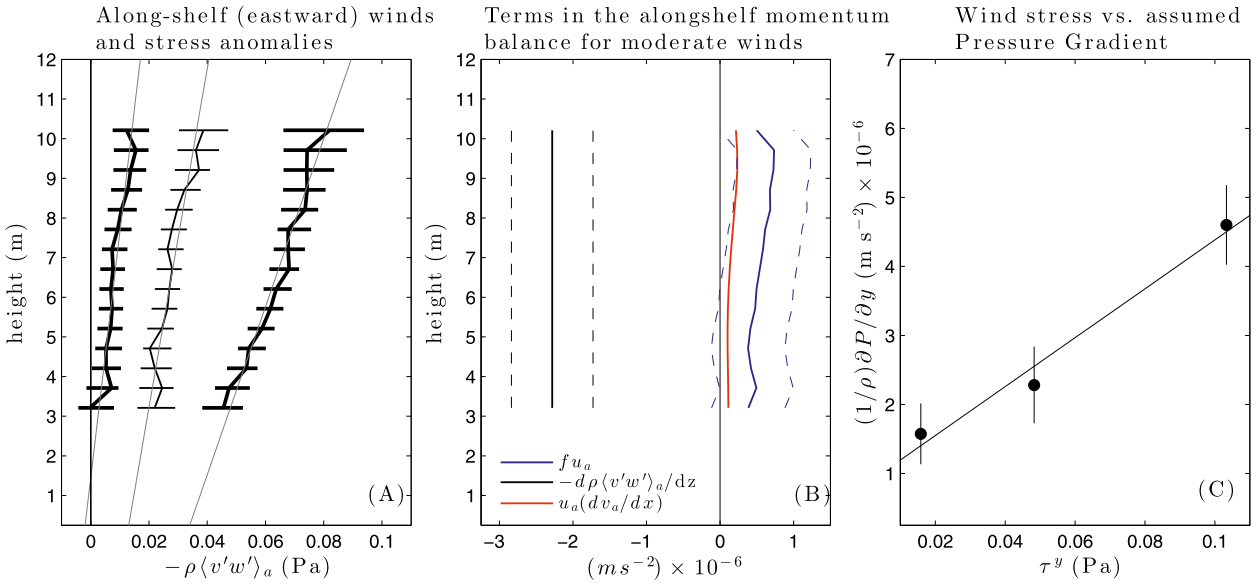

FIG. 14. Illustrating the role of pressure gradients during along-shelf wind-forcing conditions: (a) Conditionally averaged along-shelf stress anomalies for all wind stress levels during times of weak stratification with mean wind forcing shown as the matching horizontal bars near the surface and linear regressions to the stress profiles (thin lines). (b) Terms in the along-shelf momentum balance for weak stratification and moderate winds, see text for term description and methods. (c) Measured wind stress for each conditional average vs the residual momentum term for all wind levels (dots), assumed to be due to an along-shelf pressure gradient, with a linear fit shown.

270° ± 15°T, and the stratification was weak, the vertical divergence of the raw, not conditionally averaged, along-shelf stress was positively correlated with the along-shelf wind stress (Fig. 15a). A linear regression between the wind stress and vertical Reynolds stress gradient, as terms in the depth-averaged momentum equation, had a slope of 0.8 ± 0.2, similar to that described above but with reduced uncertainty. Additionally, the y intercept of the linear fit indicated a residual momentum of 3.8×10^{-6} $(\pm 1 \times 10^{-6})\,\mathrm{m\,s^{-2}}$ that was likely not related to the winds. A similar comparison using the residual across-shelf Reynolds stress vertical gradient and wind stress was also positively correlated, having a slope and y intercept of 1.2×0.25 and $1 \times 10^{-7} \pm 10 \times 10^{-7}\,\mathrm{m\,s^{-2}}$, respectively.

As seen in the stress results for weak stratification shown here, all profiles with significant along-shelf wind forcing had surface-intensified stresses, inferring the presence of an along-shelf pressure gradient, with the exception of the results from winds toward a bearing of 150°T. During wind forcing toward 150°T, which is the dominant wind direction during winter, along-shelf stresses were more uniform with depth. Fewings and Lentz (2010) found that the wind and bottom stress were the primary balance during "strong winter forcing" and thus in these conditions, inferred that the along-shelf pressure gradient was not important. This exception is not specifically representative of winter conditions or only due to weaker stratification periods, but is more likely due to the specific direction of the wind forcing from the northwest. As shown in Figs. 11d and 13f, the across-shelf, and offshore, wind is dominant in this situation, forcing a different dynamical balance than appears to occur in isolated along-shelf wind forcing.

b. What drives the mean circulation?

This work, and those that it follows (Fewings et al. 2008; Lentz et al. 2008), assume that the dynamics due to the mean background circulation and the dynamics due to wave- or wind-driven circulation can be separated by subtracting the average vertical structure during times of low waves and low winds from the average structure during times of higher wave or wind forcing. The critical aspect of this assumption is that different processes are responsible for the background circulation than are responsible for the wind- or wave-driven circulation, that is, that the mean circulation is not just the integrated, long-term response to wind or wave forcing, and that these responses are separable.

Fewings et al. (2008) and Lentz et al. (2008) assigned the mean, westward along-shelf velocity observed to the effects of either an along-shelf pressure gradient, or in summer, an across-shelf density gradient via a thermal wind balance. Mean across-shelf velocities were ascribed to the Eulerian component of the wave-driven circulation. An analysis of the observed low-wind, low-wave mean stress profiles during weak stratification together with the balance of momentum using Eqs.

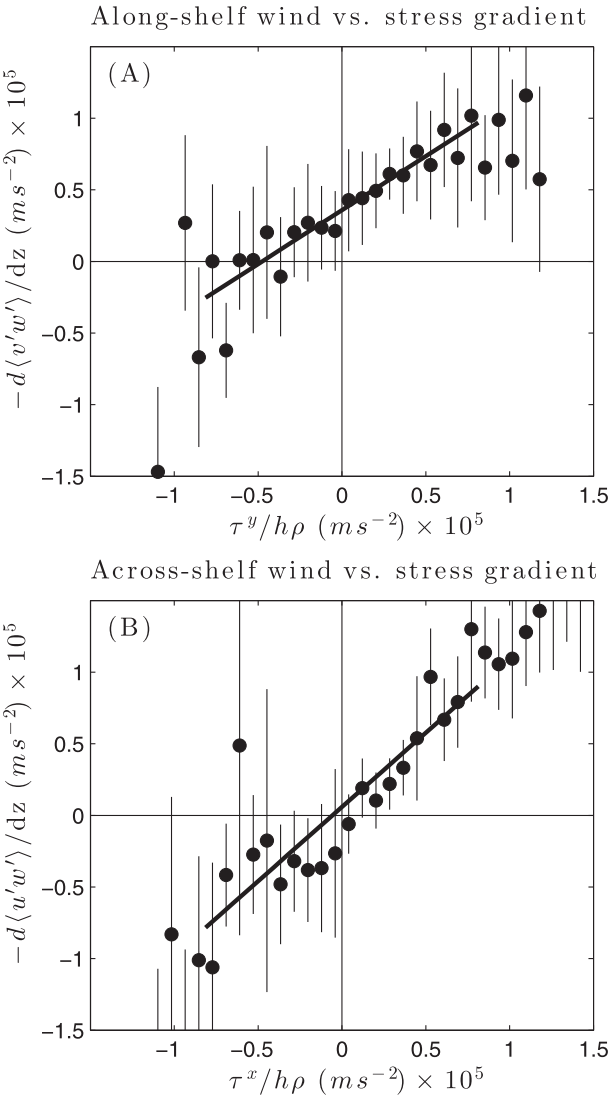

FIG. 15. (a) Along- and (b) across-shelf stresses for dominant along- or across-shelf winds and weak stratification vs the wind stress. The wind stress estimates are written in terms of the depth-averaged momentum balances. Regressions for linear fits (thick black lines) were estimated for $|\tau|/h\rho < 1 \times 10^{-5}\,\mathrm{m\,s^{-2}}$ and are given in the text.

(1a) and (1b) enable a reexamination of these conclusions. The linear fit between the along-shelf winds and stress divergence shown in Fig. 15a indicated a residual momentum of 3.8×10^{-6} ($\pm 1 \times 10^{-6}$) $\mathrm{m\,s^{-2}}$ not due to wind forcing. This residual momentum term can be accounted for by a body force such as a background along-shelf pressure gradient, as the vertical structure of the along-shelf stress profile during low winds and weak stratification increased linearly with depth to a maximum near the bottom (Fig. 8c) consistent with forcing from a barotropic pressure gradient (Fig. 2).

To test this hypothesis, the observed vertical structure of the along-shelf stress and velocity during weak winds and weak stratification was compared to that predicted by the 1D numerical model of Lentz (1995) and Lentz et al. (2008), assuming a cubic eddy-viscosity shape and forced by an along-shelf pressure gradient equivalent to the observed residual momentum present at near-zero winds. The model predicted along-shelf stress was quite similar to that observed (Fig. 8c), indicating that the inferred pressure gradient was a good fit. At higher levels of stratification, the along-shelf stress profile was still linear and bottom intensified (Figs. 8h,m), suggesting that a similar dynamical balance might drive the background along-shelf circulation at all times.

However, it is important to note that the model's similarity to the observations only shows that a depth-independent body force is responsible for driving the mean, or background circulation. Recent work by Ganju et al. (2011) found that tidal rectification could explain much of the long-term-mean depth-dependent currents in the area of the MVCO. Further, tidal stresses computed from high-resolution HF radar observations of surface currents were found to play a large role in the along-shelf momentum balance in the area of the MVCO (Kirincich et al. 2013). Thus, not all of the body force required must be due to the pressure gradient, and the sum of the along- and across-shelf tidal stresses themselves may drive a portion of the observed Reynolds stresses.

Regardless of the nature of the body force, the vertical structure of along- and across-shelf velocity were less well predicted by the model, presumably because of the differences in the observed and assumed eddy-viscosity profile (Fig. 8e). While the wave-driven response itself appears correct (Fig. 8b, thin solid gray line), the combination of the body force component of the across-shelf velocity and the wave-driven component (Fig. 8b, thin dashed gray line) has the opposite vertical structure to that observed. This difference only serves to reinforce the previous conclusions regarding the delicate nature of using the eddy-viscosity parameterizations (Lentz 1995; Kuebel Cervantes et al. 2003), and the potentially important role of stress observations in future studies.

c. *Wave-driven circulation*

For each of the wave-driven circulation profiles shown in Fig. 9, the residual wind stresses appear to fully account for the magnitude of the observed stresses, but do not account for the observed across-shelf velocity, particularly in comparison to the stresses necessary to drive a similar magnitude of across-shelf circulation by

wind or pressure forcing (Fig. 2). Thus, any stress due to the wave-driven circulation must be small, consistent with the results of Lentz et al. (2008). At higher wave heights, a more significant stress remains after accounting for that due to the wind stress. In addition, the along-shelf velocity profiles for each of these wave-height bins are vertically sheared, also in contrast to the constant velocity profiles predicted by theory (Lentz et al. 2008). However, the along-shelf velocities during isolated wave-driven flows are quite noisy, with standard deviations 3–4 times greater than the across-shelf velocities. Additional analysis (not shown here) found that this vertical structure was due to sampling issues alone. Including all velocity data in the analysis, not just those when viable stresses were present, results in vertically uniform along-shelf velocities for each of the wave-height bins. This suggests that the additional stresses seen at higher wave heights might also be due to sampling issues and are not representative of real deviations from the wave-driven flow theory.

5. Discussion and conclusions

This work represents one of the first analyses of Reynolds stresses in the coastal ocean, documenting the vertical structure of stress present during tidal-, wave-, and wind-driven forcing as well as the variable response to stratification. As wind and wave forcing are highly correlated in the coastal ocean and given the higher noise characteristics of the instruments deployed at the MVCO underwater node, conditional averages of long-term observations were utilized to separate the individual effects of each forcing type on both velocity and stress profiles at low enough uncertainty levels to enable a dynamical analysis of the results. Below, the potential biases inherent in the CF method are discussed as well as the implications of the results.

a. Methodological biases

Previous studies of the available stress estimation techniques (Stacey et al. 1999b; Lu and Lueck 1999; Williams and Simpson 2004; Kirincich and Rosman 2010) have examined the potential issues with using ADCPs to estimate Reynolds stresses. Those pertinent to the results presented above, including potential biases due to stratification, tilt, waves, and flow distortion, are described here for completeness. Regarding the effect of stratification, stress results using the CF method are effectively limited to times when the dominant size of the stress-carrying eddies are larger than the bin size (Kirincich et al. 2010). Thus, while there is no direct effect of stratification on the stress results, such as that described by Stacey et al. (1999b), the CF method may suffer from an indirect bias toward times of weaker stratification. How representative the remaining instances of larger eddy sizes are of all stratified conditions is not known. Second, while the bias due to nonzero tilt of the instrument could be significant, the correction term (appendix) appeared to reduce the mean effect of the bias enough such that the magnitude and vertical structure of the observed low-wave, low-wind stresses, where the bias due to instrument tilt issues would be the most prevalent, were consistent with a dynamical balance between the observed winds and a pressure-gradient-like body force.

Additionally, because of the noise characteristics of the mode-1 ADCP, the stress estimation method, and the covariance of winds and waves, only a small number of samples (hours of viable data) were isolated that matched a given set of conditions. As a result, the wind-driven circulation results were limited to times where $H_{sig} < 1.25$ m to ensure that the increased stresses observed at $H_{sig} < 1.4$ m (Fig. 9), occurring because of excess noise and low sample sizes, did not influence the results. While the need for this additional threshold is a limitation of the CF method, it is critical to note that viable stress estimates would not be possible at any level of wave forcing in the coastal ocean without its application. As shown by Kirincich and Rosman (2010), the CF method is the most reliable of the recently described method for the types of waves—broad banded, short period—found along the East Coast of the United States. Finally, the increases found in along-shelf velocity with depth found in the bottom-most bins during along-shelf wind forcing (Figs. 10c,d) are not characteristic of along-shelf velocity profiles due to up- or downwelling but may be the result of potential flow around the MVCO node structure itself coupled with the low sample numbers used in the conditional averaging (Table 1). Stronger flows, where the potential flow is more apparent, are more likely to lead to viable stress estimates (Kirincich et al. 2010), and thus might indirectly bias the conditionally averaged profiles.

b. Implications of the results

Despite these shortcomings, the results presented above illustrate the vertical structure of stress present during wind- and wave-forced conditions and place the changes seen during differing wind directions or increased stratification into the context of previous work only examining the velocity structure. Using the estimated stresses within the momentum balances, this work was able to infer the magnitude of the mean and fluctuating pressure gradients, finding magnitudes similar to those observed during intensive field studies

(Fewings et al. 2008) or model simulations (Wilkin 2006). As these additional observations are not always possible, this work demonstrated that use of the CF method to estimate stress distributions from ADCP observations can greatly aid smaller-scale dynamical studies in the coastal ocean.

Returning to the basic assumption in most interpretations of inner-shelf dynamics, the turbulent stress profile and its vertical divergence is thought to be the fundamental factor controlling the strength of the across-shelf circulation (Ekman 1905; Austin and Lentz 2002; Garvine 2004). When substantial turbulent stresses extend throughout the water column, the across-shelf circulation is weak. When turbulent stresses do not extend throughout the water column, perhaps because of stratification, across-shelf circulation is stronger. It has not been possible to test this assumption because direct measurements of turbulent stress profiles have not previously been possible. This has similarly hampered our understanding of the feedback process between stratification and turbulent stresses over the inner shelf.

The clearest picture of the role of stratification in altering the stress profiles comes from the results of across-shelf exchange driven by negative across-shelf, or onshore, wind forcing. As stratification increased, there was an increase in the potential exchange between weak and moderate stratification as shown by the greater velocity magnitudes near the surface and bottom in Fig. 12. Using standard methods to extrapolate the across-shelf velocity profile to the surface and bottom and compute across-shelf transport (Lentz 2001; Kirincich et al. 2005), the onshore surface transport increased from $0.05\,m^2\,s^{-1}$ during weak stratification to $0.07\,m^2\,s^{-1}$ during moderate stratification. In comparison, the across-shelf stress anomaly profiles decreased in magnitude between the two levels while the along-shelf stress component increased. The vertical structure of across-shelf velocity in the first two stratification levels were typical of inner-shelf profiles; however, the vertical structure during strong stratification level was more complex, likely having onshore flow at both the surface and bottom, and more representative of midshelf conditions where the across-shelf exchange is fully developed. At this level, downwind momentum is being transferred to the across-wind component more readily, as is evidenced by a shift in the stress vector with increased stratification (Fig. 13a). Gauging the interaction of stress, stratification, and exchange is more difficult during off-axis wind forcing, given the additional effects of the along-shelf pressure gradient on the velocity and stress vectors. Yet, the results do show that increasing stratification for forcing toward bearings of 50° and 150°T resulted in decreased stress levels and increased rotation with increasing stratification (Figs. 13e,f).

A detailed study of the observed stress and eddy-viscosity profiles can occur during periods with high data return as the confidence in the conditionally averaged results increases. The vertical structure of the conditionally averaged eddy viscosities during low winds and low waves was consistent with the vertical structure of the observed mean stress and the mean shear, particularly for higher stratifications, indicating that the conditionally averaged A_v, a noisy quantity, was accurately represented. Conditionally averaged eddy viscosities were constant over a large portion of the water column during weak stratification, but increased with depth for higher stratification. The vertical structure of eddy viscosity during the phase-averaged tidal response contrasts with that observed during mean conditions, despite both being the result of pressure gradient-like body forcings. However, the phase-averaged stress profiles observed in Fig. 7 often had a sizable nonlinear component (i.e., curvature). Thus, a significant component of the stress divergence would not be balanced by a barotropic pressure gradient. The acceleration term is significant in the phase-averaged momentum balance (not shown) and often equal and opposite to the stress divergence term throughout the water column. Thus, it is likely that the unsteady nature of tidal circulation causes the differences in eddy-viscosity profiles observed.

While these examples describe a relationship between stratification and stress, they are somewhat anecdotal, and the conditionally averaged dataset does not support the formation of a clear, concrete relationship between stress, stratification, and transport. This is particularly true during across-shelf exchange due to along-shelf wind forcing, where across-shelf (across wind) stresses were generally not significantly different from zero even during weak stratification, making a definitive test of the hypothesis out of reach. Ongoing efforts are utilizing these results to compare the dynamics shown here to that possible from a series of model parameterizations of turbulent mixing in order to build a more complete relationship between the stresses observed and the mixing and exchange present.

Acknowledgments. This work was possible due to the efforts of Janet Fredricks and the Martha's Vineyard Coastal Observatory team who have been deploying and maintaining the core instruments and infrastructure of the MVCO for over a decade. Additionally, Steve Lentz provided data from the SWWIM mooring array, which was deployed and maintained for three years by Craig Marquette. This manuscript was greatly improved by the helpful comments provided by two anonymous

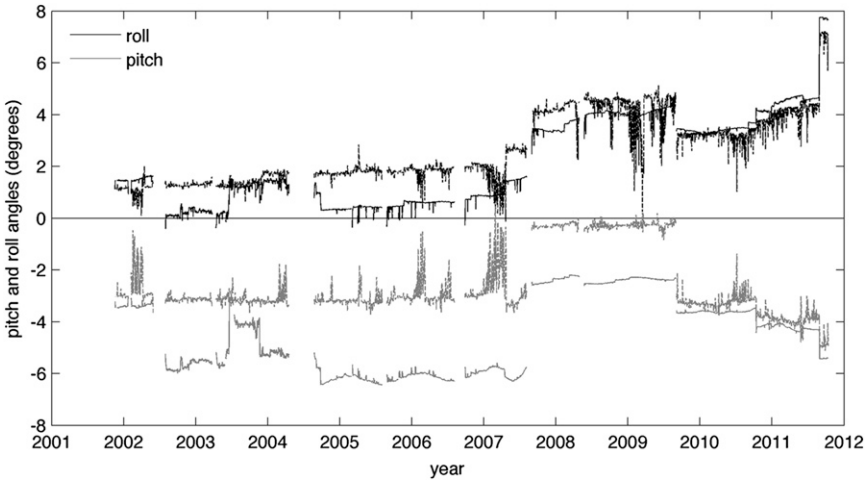

FIG. A1. The instrument-reported (solid) and externally estimated (dashed) pitch (gray) and roll (black), in degrees from vertical, for the MVCO 12-m node ADCP.

reviewers, Steve Lentz, and Thomas Connelly. The analysis was funded by the National Science Foundation under Grant OCE#1129348.

APPENDIX

Correcting for the Mean Effects of Instrument Tilt

As described by Lu and Lueck (1999) and Williams and Simpson (2004), an additional, nonwave-driven bias exists in ADCP-based estimates of stresses because of the tilt angle of the instrument relative to the vertical. For tilts greater than 2°–3°, this bias would have a noticeable effect on stress estimates, particularly for the low-magnitude stresses of interest here. However, Kirincich et al. (2010) found that effect of the mean component of the tilt-related bias, which comprises the largest part of the bias itself, could be estimated utilizing an alternative calculation of the stress close to the ADCP and assumptions about the mean anisotropy of turbulence present. The pitch and roll characteristics of the MVCO ADCPs are describe here first, followed by the methods used to estimate the correction term applied to the stress observations.

Since 2001, the pitch and roll characteristics of the MVCO ADCP have varied with both the overhauls of the node itself, as well as the tilt characteristics of the instruments deployed (Fig. A1). As described by Kirincich et al. (2010), independent estimates of the surface tilt were more accurate in explaining the observed tilt-related stress errors compared to the instrument tilts. For the full dataset used here, similar estimates of the surface tilt deviated from the instrument-recorded roll, and particularly, pitch significantly up to the fall of 2009, when a new ADCP was deployed (Fig. A1). The results identify three separate tilt periods (Table A1) which were used to transform the velocity and stress results from instrument to earth coordinates.

The bias described by Lu and Lueck (1999) and Williams and Simpson (2004) is a combined function of the tilt of the instrument relative to the principal axis of flow and the magnitude and anisotropy of turbulence. However, the tilt angle plays a dominant role as the bias follows the magnitude and sign of the tilt itself. As shown in Kirincich et al. (2010), biases near the bottom were approximately constant with increasing stress levels for the range of stresses observed at MVCO ($<1 \times 10^{-4}\,m^2\,s^{-2}$) and thus linear regressions between the near-bottom, earth-coordinate CF method Reynolds stresses and a quadratic bottom drag using the horizontal velocities from the same bin could be used to estimate the mean stress bias directly. In the full dataset examined here, estimates of the mean biases from the different levels of stratification during each separate tilt period were not significantly different from the mean biases during the period, suggesting that potential changes in anisotropy due stratification did not significantly affect the magnitude of the mean bias. Thus, estimates of mean near-bottom stress bias for each of the three major instrument tilt periods (Table A1) were assumed representative

TABLE A1. Estimates of the mean stress biases due to instrument tilt.

Tilt + period	Across-shelf stress (Pa)	Along-shelf stress (Pa)
Nov 2001–Sep 2007	−0.022 ± 0.011	0.010 ± 0.004
Sep 2007–Sep 2009	−0.019 ± 0.010	0.017 ± 0.009
Sep 2009–Nov 2011	−0.043 ± 0.026	0.016 ± 0.012

of the bulk of the instantaneous tilt-related errors at all depths and used to form the correction term applied in the text. It should be noted that the assumption of depth-independent anisotropy used in forming the correction term is only important in the analysis of the mean low-wave, low-wind stress results. Both the mean effect of the bias and the correction term itself are removed from the conditionally averaged profiles when forming the stress anomalies. The fluctuating component of the bias likely increases the scatter of the data composing the conditional averages without altering the mean value.

REFERENCES

Allen, J., and R. Smith, 1981: On the dynamics of wind-driven shelf currents. *Philos. Trans. Roy. Soc. London,* **A302,** 617–634.

Austin, J., and S. Lentz, 2002: The inner shelf response to wind-driven upwelling and downwelling. *J. Phys. Oceanogr.,* **32,** 2171–2193.

Chelton, D., 1983: Effects of sampling errors in statistical estimation. *Deep-Sea Res.,* **30,** 1083–1101.

Ekman, V., 1905: On the influence of the earth's rotation on ocean-currents. *Arkiv. Math. Astro. Fys.,* **2,** 1–53.

Feddersen, F., and A. Williams, 2007: Direct estimation of the Reynolds stress vertical structure in the nearshore. *J. Atmos. Oceanic Technol.,* **24,** 102–116.

Fewings, M., 2007: Cross-shelf circulation and momentum and heat balances over the inner continental shelf near Martha's Vineyard, Massachusetts. Ph.D. thesis, MIT–WHOI Joint Program, 267 pp.

——, and S. Lentz, 2010: Momentum balances on the inner continental shelf at Martha's Vineyard Coastal Observatory. *J. Geophys. Res.,* **115,** C12023, doi:10.1029/2009JC005578.

——, and ——, 2011: Summertime cooling of the shallow continental shelf. *J. Geophys. Res.,* **116,** C07015, doi:10.1029/2010JC006744.

——, ——, and J. Fredericks, 2008: Observations of cross-shelf flow driven by cross-shelf winds on the inner continental shelf. *J. Phys. Oceanogr.,* **38,** 2358–2378.

Ganju, N., S. Lentz, A. Kirincich, and J. Farrar, 2011: Complex mean circulation over the inner-shelf south of Martha's Vineyard revealed by observations and a high-resolution model. *J. Geophys. Res.,* **116,** C10036, doi:10.1029/2011JC007035.

Garvine, R., 2004: The vertical structure and subtidal dynamics of the inner shelf off New Jersey. *J. Mar. Res.,* **62,** 337–371.

Gerbi, G., J. Trowbridge, J. Edson, A. Plueddemann, E. Terray, and J. Fredericks, 2008: Measurements of momentum and heat transfer across the air–sea interface. *J. Phys. Oceanogr.,* **38,** 1054–1072.

Kaimal, J., J. Wyngaard, Y. Izumi, and O. Cote, 1972: Spectral characteristics of surface-layer turbulence. *Quart. J. Roy. Meteor. Soc.,* **98,** 563–389.

Kirincich, A., and J. Barth, 2009: Along-shelf variability of inner-shelf circulation along the central Oregon coast during summer. *J. Phys. Oceanogr.,* **39,** 1380–1398.

——, and J. Rosman, 2010: A comparison of methods for estimating stresses from ADCP measurements in wavy environments. *J. Atmos. Oceanic Technol.,* **28,** 1539–1553.

——, J. Barth, B. Grantham, B. Menge, and J. Lubchenco, 2005: Wind-driven inner-shelf circulation off central Oregon during summer. *J. Geophys. Res.,* **110,** C10S03, doi:10.1029/2004JC002611.

——, S. Lentz, and J. Barth, 2009: Wave-driven inner-shelf motions on the Oregon coast. *J. Phys. Oceanogr.,* **39,** 2942–2956.

——, ——, and G. Gerbi, 2010: Calculating Reynolds stresses from ADCP measurements in the presence of surface gravity waves using the cospectra fit method. *J. Atmos. Oceanic Technol.,* **27,** 889–907.

——, ——, J. Farrar, and N. Ganju, 2013: The spatial structure of tidal and mean circulation over the inner shelf south of Martha's Vineyard, MA. *J. Phys. Oceanogr.,* **43**, 1940–1958.

Kuebel Cervantes, B., J. Allen, and R. Samelson, 2003: A modeling study of Eulerian and Lagrangian aspects of shelf circulation off Duck, North Carolina. *J. Phys. Oceanogr.,* **33,** 2070–2092.

Large, W., and S. Pond, 1981: Open ocean momentum flux measurements in moderate to strong winds. *J. Phys. Oceanogr.,* **11,** 324–336.

Lentz, S., 1994: Current dynamics over the northern California inner shelf. *J. Phys. Oceanogr.,* **24,** 2461–2478.

——, 1995: Sensitivity of the inner-shelf circulation to the form of the eddy viscosity profile. *J. Phys. Oceanogr.,* **25,** 19–28.

——, 2001: The influence of stratification on the wind-driven cross-shelf circulation over the North Carolina shelf. *J. Phys. Oceanogr.,* **31,** 2749–2760.

——, R. Guza, S. Elgar, F. Feddersen, and T. Herbers, 1999: Momentum balances on the North Carolina inner shelf. *J. Geophys. Res.,* **104,** 18 205–18 226.

——, M. Fewings, P. Howd, J. Fredericks, and K. Hathaway, 2008: Observations and a model of undertow over the inner continental shelf. *J. Phys. Oceanogr.,* **38,** 2341–2357.

Lu, Y., and R. Lueck, 1999: Using a broadband ADCP in a tidal channel. Part II: Turbulence. *J. Atmos. Oceanic Technol.,* **16,** 1568–1579.

Mellor, G. L., and T. Yamada, 1982: Development of a turbulence closure model for geophysical fluid problems. *Rev. Geophys.,* **20,** 851–875.

Mitchum, G., and A. Clarke, 1986: The frictional nearshore response to forcing by synoptic scale winds. *J. Phys. Oceanogr.,* **16,** 934–946.

Munchow, A., and R. Chant, 2000: Kinematics of inner shelf motions during the summer stratified season off New Jersey. *J. Phys. Oceanogr.,* **30,** 247–268.

Nidzieko, N., D. Fong, and J. Hench, 2006: Comparison of Reynolds stress estimates derived from standard and fast-ping ADCPs. *J. Atmos. Oceanic Technol.,* **23,** 854–861.

Pawlowicz, R., B. Beardsley, and S. Lentz, 2002: Classical tidal harmonic analysis including error estimates in MATLAB using T_TIDE. *Comput. Geosci.,* **28,** 929–937.

Rosman, J., J. Hench, J. Koseff, and S. Monismith, 2008: Extracting Reynolds stresses from acoustic Doppler current profiler measurements in wave-dominated environments. *J. Atmos. Oceanic Technol.,* **25,** 286–306.

Roughgarden, J., S. Gaines, and H. Possingham, 1998: Recruitment dynamics in complex life cycles. *Science,* **241,** 1460–1466.

Shaw, W., and J. Trowbridge, 2001: The direct estimation of near-bottom turbulent fluxes in the presence of energetic wave motions. *J. Atmos. Oceanic Technol.,* **18,** 1540–1557.

Stacey, M., S. Monismith, and J. Burau, 1999a: Measurements of Reynolds stress profiles in unstratified tidal flow. *J. Geophys. Res.,* **104** (C5), 10 933–10 949.

——, ——, and ——, 1999b: Observations of turbulence in a partially stratified estuary. *J. Phys. Oceanogr.,* **29,** 1950–1970.

Tilburg, C., 2003: Across-shelf transport on a continental shelf: Do across-shelf winds matter? *J. Phys. Oceanogr.,* **33,** 2675–2688.

Trowbridge, J., 1998: On a technique for measurement of turbulent shear stress in the presence of surface waves. *J. Atmos. Oceanic Technol.,* **15,** 290–298.

Warner, J., C. Sherwood, H. Arango, and R. Signell, 2005: Performance of four turbulence closure models implemented using a generic length scale method. *Ocean Modell.,* **8,** 81–113.

Wilcox, D., 1988: Reassessment of the scale-determining equation for advanced turbulence models. *Amer. Inst. Aeron. Astron. J.,* **26,** 1299–1310.

Wilkin, J., 2006: The summertime heat budget and circulation of Southeast New England Shelf waters. *J. Phys. Oceanogr.,* **36,** 1997–2011.

Williams, E., and J. Simpson, 2004: Uncertainties in estimates of Reynolds stress and TKE production rate using the ADCP variance method. *J. Atmos. Oceanic Technol.,* **21,** 347–357.

Xu, Z., and A. Bowen, 1994: Wave- and wind-driven flow in water of finite depth. *J. Phys. Oceanogr.,* **24,** 1850–1866.